Activation and clonal expansion of CD8^{+}T cells in patients with anti-NMDAR encephalitis revealed by single-cell RNA sequencing analysis

Sisi Li[1,2a], Xiang Hu[3a], Yi Yang[1], Jierui Wang[1], Zihua He[1], Luoting Yu[1], Zhen Hong[1], Dong Zhou[1*], Jinmei Li[1*]

[1] Department of Neurology, West China Hospital, Sichuan University, No. 37 Guoxue Road, Chengdu, Sichuan 610041, People's Republic of China
[2] Department of Breast Cancer, Chongqing University Cancer Hospital, Chongqing, 400030, China
[3] State Key Laboratory of Biotherapy, West China Hospital, Sichuan University, Chengdu, 610041, China

[a]These authors contributed equally to this work.

Corresponding author:
Jinmei Li, MD, Ph.D.
Department of Neurology, West China Hospital, Sichuan University
No. 37 Guoxue Road, Chengdu, Sichuan 610041, People's Republic of China
Email:lijinmei@wchscu.cn
Fax and Tel: 86-028-85422549

Dong Zhou, MD, Ph.D.
Department of Neurology, West China Hospital, Sichuan University
No. 37 Guoxue Road, Chengdu, Sichuan 610041, People's Republic of China
Email: zhoudong66@yahoo.de
Fax and Tel: 86-028-85422549

Abstract

Background: Anti-N-methyl-D-aspartate receptor encephalitis (NMDAR-E) is a rare and severe form of antibody-mediated autoimmune encephalitis. While the roles of B cells and NMDAR antibodies in NMDAR-E have been extensively studied, the contribution of T cell subsets to the development of the disease remains unclear.

Methods: We utilized single-cell RNA sequencing (scRNA-seq) and single-cell TCR sequencing (scTCR-seq) to examine a comprehensive collection of 45,088 individual immune cells sourced from both NMDAR-E patients and control subjects. Besides, we incorporated 14,536 immune cells obtained from a publicly available database. Additionally, cytometry analysis was conducted on samples from 60 NMDAR-E patients (with 89 samples) and 44 individuals in the control group. To investigate the influence of $CD8^+$T cells on B cells, we performed in vitro co-culture experiments.

Results: We observed the activation of effector memory $CD8^+$T cells in the CSF and peripheral blood (PB) of NMDAR-E patients, accompanied by an expansion of TCR clones. These clonal $CD8^+$T cells exhibited upregulated gene expression associated with cytotoxicity and cell trafficking. Furthermore, we detected elevated levels of KIR^+CD8^+T cells in the CSF and PB of NMDAR-E patients. Cell communication analysis revealed that these inhibitory KIR^+CD8^+T cells could interact with B cells through MHC-I molecules. Surprisingly, $CD8^+$T cells isolated from the PB of NMDAR-E patients induced autologous B cell death, resulting in a higher rate of B cell apoptosis compared to the control group.

Conclusion: Activated $CD8^+$T cells with TCR clones in NMDAR-E patients may contribute to the pathogenesis of NMDAR-E.

Keywords: Anti-NMDAR encephalitis; single-cell RNA sequencing; single-cell TCR sequencing; $CD8^+$T cells; KIR^+CD8^+T cells

Abbreviations[1]

[1] NMDAR: Anti-N-methyl-D-aspartate receptor; CBA: cell-based assay; CNS: central nervous system; CSF: cerebrospinal fluid; PBMCs: Peripheral blood mononuclear cells; PB, peripheral blood; scTCR-Seq: single-cell TCR sequencing; scRNA-seq: Single cell RNA sequencing; Temra:$CD45RA^+$ effector memory T cells; Tem: effector memory T; Tcm: central memory T; Tn: naïve T; HC: Healthy control; IIH: Idiopathic intracranial hypertension; Bm: memory B cells; Bn, naïve B cells; ASCs: Antibody-secreting cells; DN, CD27-IgD-double negative B cells; t-SNE: t-distributed neighbor embedding; MHC: Major histocompatibility complex; DEGs: Differentially expressed genes; KIRs: killer-cell immunoglobulin-like receptors; KEGG: Kyoto Encyclopedia of Genes and Genomes pathway.

1. Introduction

Anti-N-methyl-D-aspartate receptor (NMDAR) encephalitis (NMDAR-E) is a rare and severe autoimmune encephalitis of the central nervous system (CNS) caused by autoantibodies targeting the GluN1 subunit of the receptor [1, 2]. It is characterized by diverse clinical manifestations, including rapid progression of psychiatric symptoms, cognitive impairment, epileptic seizures, atypical movements, or unexplained coma [3, 4]. Despite first-line immunotherapy with steroids, plasma exchange, and intravenous immunoglobulin, approximately 20% of patients show no response [5-7]. A substantial proportion, around 75%, requires intensive care unit treatment[3, 8], and a recurrence risk of 20-25% is observed [7, 8]. Moreover, long-term morbidity, such as persistent cognitive deficits, affects almost all patients [9]. Consequently, a comprehensive understanding of NMDAR encephalitis pathogenesis is imperative to enhance future treatment strategies.

Although it is widely believed that B cells and autoantibodies play a significant role in the pathogenesis of anti-NMDAR encephalitis [10-12], recently emerging evidence suggests the potential involvement of T cell subsets in its development. Elevated levels of T cell-related cytokines, including interleukin-6 (IL-6), IL-17, interferon-gamma (IFN-γ), and tumor necrosis factor-alpha (TNF-α), have been detected in the cerebrospinal fluid (CSF) of NMDAR-E patients [13-15]. Analysis of brain samples from biopsies or autopsies has revealed the infiltration of T cells, B cells, and plasma cells in the brain parenchyma and perivascular spaces of NMDAR-E patients [16-18]. Notably, Jones et al. established an active immunization mouse model of anti-NMDAR encephalitis, which demonstrated T cell infiltration in critical brain areas [19]. Moreover, TCRa cell knockout resulted in the disappearance of clinical symptoms and increased survival rate in mice, indicating the potential significance of mature T cells in anti-NMDAR encephalitis[19]. Recently, a study constructed a humanized mouse model by transferring patient peripheral blood mononuclear cells (PBMCs) into mice, revealing the infiltration of $CD8^+$T cells in the hippocampus[20].

However, the potential alterations in T cell subpopulations, as well as their transcriptomic and immunological characteristics, in the CSF and peripheral blood of NMDAR-E patients remain unknown. In this study, a comprehensive approach employing single-cell RNA sequencing (scRNA-seq), single-cell TCR sequencing (scTCR-seq), flow cytometry, and in vitro cell co-culture was conducted to investigate T cell phenotypes, TCR clonality, and the potential contribution of T cell subsets to anti-NMDAR encephalitis in patients (Fig. 1A).

2. Methods

2.1 Selection of Patients and Controls

All samples were collected from West China Hospital, Sichuan University between October 2019 and February 2023. The research conducted in this study received ethical approval from the Institutional Review Board (IRB) of West China Hospital,

under the protocol number ChiCTR1900027074. Prior to their involvement, all participants provided written informed consent. This study adheres to the ethical guidelines outlined in The Code of Ethics of the World Medical Association (Declaration of Helsinki).

2.1.1 Inclusion criteria of patients and control samples

The inclusion criteria for NMDAR-E were established as follows: (1) Patients diagnosed with NMDAR-E according to the latest consensus statements[1], demonstrating one or more of the eight primary symptoms, including psychiatric symptoms, memory loss, speech dysfunction, seizures, movement disorders, altered consciousness, autonomic dysfunction, and central hypoventilation. Additionally, patients who tested positive for NMDAR antibodies in CSF using a cell-based assay (EUROIMMUN, Lübeck, Germany), and patients who have reasonably excluded other diseases; (2) Patients who agree to participate in the study; and (3) Patients who have obtained sufficient CSF or blood samples.

Inclusion criteria for the control group CSF samples are as follows: (1) negative CSF examination results, including routine, biochemical, and IgG tests, as well as negative bacterial, fungal and viral tests; (2) autoantibodies, demyelinating antibodies, and antibodies associated with paraneoplastic syndromes in CSF should all be negative; (3) the cranial magnetic resonance imaging should not reveal any signs of inflammation; (4) patients should be in good physical health; and (5) the final diagnosis should be idiopathic intracranial hypertension, chronic headache, anxiety or other conditions without organic changes.

The peripheral blood control group samples are healthy adult volunteers who are matched with the age and gender of the included patients.

2.1.2 Exclusion criteria of patients

The exclusion criteria consist of the following: (1) laboratory evidence indicating patients with infectious encephalitis, such as viral infection (TORCH IgM), bacterial infection (CSF smear and culture), tuberculosis (acid-fast staining), parasitic infection (antibody detection), or fungal and cryptococcal meningitis (CSF smear, culture, and ink staining); (2) a history of other autoimmune diseases, including rheumatoid arthritis, type I diabetes, and systemic lupus erythematosus; (3) other severe neurological disorders, such as acute demyelinating encephalomyelitis, dementia, stroke, and Parkinson's disease; (4) patients with other antibodies linked to autoimmune encephalitis or neurological paraneoplastic syndrome antibodies (Table e-1); and (5) Patients in the acute phase of the disease were excluded if they had received treatment with steroids or immunosuppressive agents. Similarly, patients in the relapse or remission phase were excluded if they had received these drugs within one month prior to the sampling.

2.1.3 Sample information for single cell analysis and flow cytometry

This study investigated scRNA-seq and scTCR-seq analyses using samples from nine subjects, consisting of three CSF samples from NMDAR-E patients, four PBMC samples from NMDAR-E patients, and two PBMC samples from control groups. In addition, six CSF control samples from idiopathic intracranial hypertension (IIH) were obtained from the public dataset GSE138266 and were exclusively used for scRNA-seq analysis (Table e-2).

Flow cytometry was used to detect changes in T-cell subsets in the CSF and PBMC of patients with NMDAR-E as well as in the control group. The following analyses were conducted: (1) a total of 25 CSF samples were analyzed using flow cytometry, including 15 samples from NMDAR-E patients and 12 samples from control individuals (age: 29.26±9.25 vs. 30.9±10.9; male proportion: 53.3% vs. 58.3%) (Table e-3); (2) Flow cytometry was used to analyze T cell subsets in 34 PBMC samples from NMDAR-E patients and 21 healthy controls (age: 31.76±11.56 vs. 26.57±3.09; male proportion: 52.9% vs. 57.1%) (Table e-4); and (3) $KIR^{+}CD8^{+}T$ cell subsets were analyzed in samples from 9 severe (age: 39.8±14.0, male proportion: 66.7%), 10 mild to moderate (age: 29.7±12.4, male proportion: 50.0%), 13 recurrent (age: 37.8±18.4, male proportion: 46.2%), and 8 remitting NMDAR-E patients (age: 26.6±12.0, male proportion: 62.5%), as well as 11 controls (age: 27.18±3.28, male proportion: 63.6%) (Table e-5). Please note that in this study, during the analysis of T cell subpopulations using flow cytometry, 19 samples from panel (3) (severe group and mild/moderate group) were sourced from the same group of patients as the samples from panel (2). Furthermore, 10 CSF samples from panel (1) and PBMC samples from panel (2) were obtained from the same patient cohort. Thus, the study included a total of 60 NMDAR-E patients (consisting of 89 samples) and 44 control group patients.

2.2 Data collection

The relevant data was collected by reviewing the medical records of NMDAR-E patients. Demographic information such as sex, age, and age at disease onset was recorded. Clinical data included symptoms such as abnormal psychiatric symptoms, cognitive dysfunction, seizures, memory deficits, movement disorders, disturbances of consciousness, and central hypoventilation. The titers of NMDAR antibodies in the CSF and serum, therapy details, and modified Rankin Scale (mRS) scores at the time of sample collection were also documented. Disease severity was assessed using the mRS scores [21], where a score of <3 indicated mild illness and ≥3 indicated moderate/severe illness. Relapse was defined as the recurrence or emergence of new symptoms after a period of at least 2 months marked by clinical stabilization or improvement[22].

2.3 Collection and processing of CSF and peripheral blood

Peripheral blood samples (4-5 mL) were obtained from both NMDAR-E patients and control groups. To isolate PBMCs, Ficoll-Paque medium (Ficoll Paque Plus, GE Healthcare) was used for density gradient centrifugation. After separation, PBMC samples were preserved by freezing them overnight at -80°C and subsequently

transferring them to liquid nitrogen for long-term storage. These samples were later used for scRNA-Seq, scTCR-seq, and flow cytometry analysis.

We collected CSF samples from both NMDAR-E patients and control groups via lumbar puncture. Fresh CSF samples of 15-30 mL were required for scRNA-seq and scTCR-seq analysis, while 5-10 mL of fresh CSF samples were needed for flow cytometry analysis. Sample processing was conducted within 2 hours after collection.

2.4 Flow cytometry

PBMCs and CSF cells were suspended in phosphate-buffered saline (PBS) supplemented with 10% fetal calf serum (FCS). Careful handling of all samples was ensured by keeping them on ice or at a temperature of 4 to protect them from direct light exposure. Flow cytometry experiments were performed using the LSRFortessa flow cytometer from BD Biosciences. An antibody panel consisting of eight different fluorescent dyes was prepared to characterize T cell subsets in CSF and PBMC cells. The panel included the following antibodies: CD3-BV605, CD8-APC-Cy7, CD4-PerCP-Cy5-5, TCRδ1-FITC, TCRδ2-BV421, CD45RA-BV786, and CCR7-FITC. To analyze $KIR^{+}CD8^{+}T$ cells in PB, the following antibodies were used: CD3-BV605, CD8-APC-Cy7, CD45RA-BV786, CCR7-FITC, CD158b-PerCP-Cy5-5, and CD158e-PE. For the separation of $CD8^{+}T$ cells and B cells, the following antibodies were employed: CD3-BV605, CD8-APC-Cy7, 7AAD-PerCP-Cy5-5, and CD19-BV785. In vitro co-culture of $CD8^{+}T$ cells and B cells, as well as measurement of B cell apoptosis, were detected using the following antibodies: CD3-BV605, CD19-BV785, CD38-APC, CD27-PE-Cy7, IgD-APC-Cy7, AnnexinV-PE, and 7AAD-PerCp-Cy5-5. For each experiment, control samples were stained separately and left unstained. A compensation matrix was developed to facilitate analysis using FlowJo software (v. 10.5.3, FlowJo LLC, BD). Detailed information for each flow cytometry antibody can be found in Table e-6.

2.5 Single-cell RNA-Seq data analysis

2.5.1 Data processing, quality control, and batch correction strategies

The raw data underwent processing utilizing CellRanger software (version 7.0.0) and aligned with the GRCh38 human reference genome. The gene-barcode matrix was analyzed using Seurat package in R (version 4.2.0). During the quality control process, cells with less than 200 detected genes for environmental RNA, cells with mitochondrial gene expression total exceeding 15% for dead cells, and doublets identified by Scrublet (Python 3.7.3) were excluded. In order to mitigate the impact of batch effects, the single-cell variational inference (scVI) method was employed to integrate expression data from different samples [23]. scVI is a powerful deep generative model that enables the learning of a probabilistic representation of the transcriptional states of single cells while accounting for sequencing batches. Due to its ability to implicitly correct for batch effects, there is no need for batch correction steps [24].

2.5.2 Identification of cell cluster

To perform principal component analysis (PCA), we utilized Seurat's RunPCA function to select the top 2000 features displaying the most significant expression differences between cells. Subsequently, cell clustering was performed on the top 30 dimensions using the FindClusters function. The resulting clusters were visualized using t-distributed stochastic neighbor embedding (t-SNE), and the identification of cell types within each cluster was determined based on characteristic marker genes.

After conducting quality control and technical noise adjustment, a total of 45,088 single-cell transcriptomic profiles were included for analysis. Additionally, we incorporated 14,536 CSF cells from six idiopathic intracranial hypertension (IIH) patients obtained from a publicly available database as control samples. Detailed gene expression levels for each group can be found in eFig.1A and Table e-7. By employing t-SNE and examining the expression of characteristic marker genes, we successfully identified eight immune cell subpopulations and visualized their distribution in the dimension reduction plots (eFig.1B and eFig.1C). T cells were found to be the predominant immune cell type observed in both the CSF and PB of the patients. Additionally, B cells, monocyte/macrophages, and dendritic cells were detected in these samples (eFig.1D). Previous unpublished research by our team provided detailed explanations of B cell phenotypes in the CSF and PB of NMDAR-E patients. Consequently, this study primarily focuses on investigating the composition of T cell subpopulations and transcriptomic changes. As NK cells share similar gene markers with some $CD8^{+}$T cells, further identification will be conducted in the subsequent stage to distinguish T cell subpopulations from NK cell subpopulations.

2.5.3 T/NK cell clustering analysis

For the T/NK cell clustering analysis, we utilized t-tests and beta-binomial generalized linear models from the aod::betabin package. These methods allowed us to examine differences in cluster abundance, measured as cell counts, between NMDAR-E encephalitis and control donors[24].

2.5.4 DEGs and pathway analysis

To identify genes exhibiting differential expression (DEGs), we employed Seurat's "FindMarkers" or "FindAllMarkers" functions. In addition, we utilized the Wilcoxon test to assess the significance of gene expression differences. Genes expressed in at least 25% of the cells within the target cluster were considered, and a p-value threshold below 0.05 was used to determine statistical significance. To visualize the expression patterns of specific genes, we generated violin plots using the Seurat package. Furthermore, we conducted trajectory analysis by employing diffusion mapping for dimensionality reduction and the Potential of Heat-diffusion for Affinity-based Transition Embedding (PHATE) algorithm[25]. For the enrichment analysis of the identified DEGs in the Kyoto Encyclopedia of Genes and Genomes (KEGG), we utilized the singleseqgset package (https://github.com/arc85/singleseqgset).

2.5.5 Cell communication

To investigate the intercellular interactions between $KIR^{+}CD8^{+}T$ cell and B cell clusters in NMDAR-E patients and controls, we employed the R package CellChat. This package facilitated the identification and visualization of intercellular communication by leveraging known ligand-receptor pairs[26]. The CellChat package can be accessed at https://github.com/sqjin/CellChat.

To explore the interactions between potential ligands and receptors, we analyzed the relative expression levels across different cell types using CellPhoneDB (v3.0.1) (www.CellPhoneDB.org). Heatmaps and bubble plots were generated using the ktplots (v1.2.1) R package to visualize these interactions.

2.6 Analysis of single-cell TCR sequencing data

The study utilized Cell Ranger software (version 6.0.1) to identify CDR3 sequences and rearranged TCR genes in the 10x Genomics dataset. The α-β pairing within the framework was considered to determine the dominant TCRs and unique clone types. Clonal populations were denoted by the presence of a clone type in at least two cells, and clonality was determined by the number of cells with the same dominant α-β pairing. Clonotypes were divided into three groups based on the number of T cells expressing the same TCR: ">=3", "2", and "1". Following a similar approach as described in previous studies[27, 28], we employed a statistical method to assess the sharing of TCR clones based on TCR clonotypes between different clusters. Specifically, to evaluate the sharing of TCR clones in both the NMDAR-E patient CSF and PB datasets, we generated a table for each pair of clusters and computed the number of clone types shared among cells within the same cluster or across different clusters.

2.7 In vitro experiments

The PBMCs of NMDAR-E patients and controls were prepared, and $CD8^{+}T$ cells and B cells were sorted by flow cytometry and co-cultured at a ratio of $CD8^{+}T$: B cells (5:1). After 96 hours of cultivation, flow cytometry antibody staining was performed, incubated at 4□ in the dark for half an hour, then washed, resuspended, and filtered into flow tubes. The LSRFortessa flow cytometer (BD Biosciences) was used for detection.

2.8 Live cell imaging

After sorting $CD8^{+}T$ and B cells from PBMCs of NMDAR-E patients and healthy controls using flow cytometry, $CD8^{+}T$ cells were stained with Calcein Green (Invitrogen, USA) and co-cultured with B cells. Propidium iodide (PI) dye (red; Invitrogen, USA) was added to the culture medium. The direct contact time between $CD8^{+}T$ cells and B cells, as well as target cell apoptosis, were observed using confocal microscopy.

2.9 Statistical analysis

Descriptive analysis was performed to examine the sociodemographic and clinical data, and the results were expressed as percentages or means using IBM SPSS Statistics version 22.0 (IBM Corp., Armonk, NY, USA). The flow cytometry analysis

was conducted using FlowJo software (v. 10.5.3, FlowJo LLC, BD). Graphs were generated using GraphPad Prism (V.9.0). To assess the differences between cell subpopulations in the two groups, an unpaired t-test was employed. To facilitate image layout, we utilized the commercial software Adobe Illustrator 2020. We described sample sizes and statistical tests methods in the figure legends to provide a comprehensive understanding of the results. Unless otherwise specified, P-values or adjusted P-values less than 0.05 were considered significant.

3. Results

3.1 T Cell Subset Composition and Phenotypic Characteristics in the CSF and PB of NMDAR-E Patients

In this study, we employed t-SNE analysis to visualize T cell subsets and natural killer (NK) cells derived from the CSF and PB of both NMDAR-E patients and control subjects. The total number of T/NK cells analyzed was 47,922 (Fig. 1B). To classify different T cell subpopulations, we employed marker genes and identified distinct clusters (Fig. 1C and eFig.2A). Naïve $CD4^+$T cells ($CD4^+$Tn) and naïve $CD8^+$T cells ($CD8^+$Tn) were identified based on the high expression of *CCR7*, *SELL*, and *LEF1* genes, whereas memory $CD4^+$T cells ($CD4^+$Tm) exhibited lower expression levels of these genes. Effector memory $CD8^+$T cells ($CD8^+$Tem) were identified based on cytotoxic genes such as *NKG7*, *GZMK*, and *PRF1*, while central memory $CD8^+$T cells ($CD8^+$Tcm) expressed *IL7R* and *TCF7*. Effector $CD8^+$T cells ($CD8^+$Te) were distinguished by marker genes like *NKG7* and *GNLY*. Additionally, we identified γδT cell clusters using *TRDV2* and *TRGV9* markers.

Next, we compared the changes in T cell subsets in the CSF and PB between NMDAR-E patients and control subjects. Naïve T cells were predominant in the PB, whereas memory T cells were more prevalent in the CSF (eFig.2B). Specifically, NMDAR-E patients exhibited a significant increase in $CD8^+$Tem and γδT subsets in the PB compared to the control group, while $CD4^+$Tn clusters showed a significant decrease in these patients (Fig.1D). In the CSF, NMDAR-E patients demonstrated significantly higher levels of effector $CD8^+$T cells (including $CD8^+$Te and $CD8^+$Tem cells) and γδT cells compared to the IIH group (Fig.1E). The composition of T cell subsets in the CSF and PB of NMDAR-E patients is also different (Fig.1F). Pseudo-time maturation trajectory analysis revealed the differentiation of $CD8^+$T clusters in NMDAR-E patients from $CD8^+$Tn cells into $CD8^+$Te and $CD8^+$Tem cells (eFig.2C).

3.2 Activation of Cytotoxic $CD8^+$T Cells in the CSF and PB of NMDAR-E Patients

We used flow cytometry to analyze alterations in T cell subsets in the CSF of 15 NMDAR-E patients and 12 controls. Our results revealed a remarkable elevation in the population of $CD45RA^+$ effector memory $CD8^+$T cells ($CD8^+$Temra) in the CSF of NMDAR-E patients (Fig.2A, Fig.2B, and eFig.3A). Conversely, no significant difference was observed in the levels of $CD4^+$T cell subsets between the two groups (Fig.2C, Fig.2D, and eFig.3B).

Transcriptomic analysis of CSF T cell subsets indicated upregulated DEGs in effector $CD8^+$T cells, including $CD8^+$Tem and $CD8^+$Te, in NMDAR-E patients. These cells exhibited characteristics associated with tissue residence, cytotoxicity, co-inhibitory molecules, TH1 response, IFN-driven transcripts, and TCR signaling when compared to the control group (Fig.2E and eFig.4). For instance, the tissue residence of T cells was influenced by the upregulation of genes such as *CXCR6*, *CD69*, *PRDM1*, and *LGALS3* in NMDAR-E patients[29]. Regarding cytotoxicity, NMDAR-E patients displayed elevated expression of genes such as *GZMB*, *GNLY*, *GZMK*, and *PRF1*[29, 30]. Furthermore, NMDAR-E patients showed upregulation of genes involved in TCR signaling, such as *GIMAP1*, *GIMAP4*, *GIMAP5*, and *GIMAP6* [28]. Additionally, KEGG pathway analysis revealed enrichment of DEGs in effector $CD8^+$T cells in pathways such as T cell receptor signaling pathway, cellular senescence, natural killer cell-mediated cytotoxicity, and chemokine signaling pathway (Fig.2F).

We next analyzed peripheral T cell subsets of 34 patients and 21 control subjects using flow cytometry. The results showed that $CD8^+$Temra and $CD8^+$Tem cell levels were significantly elevated in NMDAR-E patients compared to controls, while $CD8^+$Tcm cell levels were lower in patients (Fig.3A, Fig.3B, and eFig.3C). Similar to the CSF analysis, no significant statistical differences were observed in the levels of $CD4^+$T cell subsets between the two groups (Fig.3C, Fig.3D, and eFig.3D). Differential expression analysis revealed that $CD8^+$Te and $CD8^+$Tem cells in the PB of NMDAR-E patients exhibited significant cytotoxic features, including the expression of *NKG7*, *GZMB*, and *GNLY* [29] (Fig.3E, Fig.3F, and eFig.5). Additionally, upregulation of ITGA4 and ITGB1 genes, involved in T cell entry into the CNS[31], were observed in $CD8^+$Te and Treg cells in the PB of NMDAR-E patients (Fig.3G). In addition to cytotoxicity and TCR signaling pathways, the KEGG enrichment analysis of DEGs in periphery T cell subsets of NMDAR-E patients showed enrichment in MAPK, TNF, and cell apoptosis signaling pathways (Fig.3H). Furthermore, as well as in relapsing NMDAR-E patients compared to the control group (Fig.3K and Fig.3L). Analysis of T cell subsets by both scRNA-seq and flow cytometry supports the activation of $CD8^+$T cells in the CSF and peripheral blood of NMDAR-E patients.

3.3 TCR Clonal Expansion of $CD8^+$T Cells in the CSF and blood of NMDAR-E patients

The TCR sequences of individual T cells are inherently unique, and clonal expansion occurs when T cells recognize specific antigens [32]. By employing scTCR-seq, we observed a significant increase in TCR clone expansion in the PB of NMDAR-E patients compared to the control group. Notably, the expansion of TCR clones in the CSF of patients was even more pronounced than in the PB (Fig.4A and Fig.4B). Generally, naive T cell clusters ($CD4^+$Tn and $CD8^+$Tn) and $CD8^+$Tcm and Treg subsets exhibited limited clonal expansion. Conversely, highly expanded clones (TCR clones≥3) are primarily concentrated in $CD8^+$Te, $CD8^+$Tem, $CD4^+$Tm, and MAIT clusters (Fig.4C-E).

In the CSF of patients, $CD8^+$T cells with TCR clones exhibited upregulation of genes associated with cytotoxicity (*GZMA* and *GZMK*)[30] and cell trafficking (*CCL5*, *CCL4*, *CCL4L2* and *ITGB1*) [33], while showing downregulation of genes associated with naïve/memory (*CCR7* and *SELL*) (Fig.4G and Fig.4H). Similarly, clonal $CD8^+$T cells in the blood of patients exhibited upregulation of genes linked to cytotoxicity (*GZMH*, *GZHB* and *PRF1*) and cell trafficking (*CX3CR1* and *ITGB1*) [33] (Fig.4F and Fig.4H).

In NMDAR-E patients, the group with TCR clone numbers ≥ 3 in both CSF and PB demonstrated significantly DEGs compared to groups with clone numbers of "2" and "1" (eFig.6). Furthermore, we identified numerous shared TCR clone sequences among T cell subgroups in both the CSF and PB of NMDAR-E patients. For instance, the sharing of TCR clones was more pronounced between $CD4^+$Tn and $CD8^+$Tn in the PB of patients and between $CD4^+$Tn and $CD4^+$Tm, as well as between $CD4^+$Tm and $CD8^+$Tem in the CSF (Fig.4I and Fig.4J).

3.4 Alterations in KIR^+CD8^+T cell levels and transcriptional features of NMDAR-E patients

In this study, we investigated the presence and characteristics of a regulatory subset of $CD8^+$T cells known as KIR^+CD8^+T cells in NMDAR-E patients. These cells express killer-cell immunoglobulin-like receptors (KIRs), which possess inhibitory functions contributing to their regulatory role [33, 34]. Importantly, KIR^+CD8^+T cells have been shown to suppress pathogenic $CD4^+$T cells in autoimmune and infectious diseases [33].

Our analysis revealed a notable rise in the proportion of $CD8^+$T cells expressing inhibitory KIRs, specifically KIR3DL1 and KIR2DL3, in both the CSF and blood of NMDAR-E patients (Fig.5A and Fig.5B). These KIR^+CD8^+T cells were predominantly activated $CD8^+$T cells including $CD8^+$Te, $CD8^+$Tem, and $CD8^+$Tm cells (Fig.5C). To further analyzed the KIR^+CD8^+T cell subset, we analyzed an additional 40 NMDAR-E patients (9 severe, 10 mild/moderate, 13 relapsed, and 8 in remission) and compared them to 11 healthy controls. Although the statistical difference was not significant, we observed higher levels of $CD158e^+$ (KIR3DL1) $CD8^+$T cells in the severe group compared to the control group (Figure 5D, Figure 5E, and eFig.7A). Additionally, we noticed a significant increase in the levels of $CD158e^+CD8^+$Temra cells in the PB of severe and relapsed groups when compared to the remission and control groups (Figure 5F and Figure 5G). Moreover, within the $CD8^+$Temra cell subset, we observed a higher presence of CD158e-positive cells in the PB of severe patients compared to the control group (eFig.7B-D).

The analysis of scTCR-seq data showed notable TCR clonality in KIR^+CD8^+T cells present in both the PB and CSF of NMDAR-E patients (Fig.5H). Additionally, more than one-third of KIR^+CD8^+T cells exhibited highly expanded TCR clone numbers (≥3) in the CSF (Fig.5I). Comparing KIR^+CD8^+T cells with and without TCR clones in NMDAR-E patients, we found that KIR^+CD8^+T cells with TCR clones in the PB overexpressed genes related to cytotoxicity (*GZMB* and *GNLY*) [33] and cell

trafficking, while the expression of genes associated with naive/memory markers decreased (Fig.5J). The upregulated DEGs in clonal KIR^+CD8^+T cells in both the CSF and PB of NMDAR-E patients are significantly enriched in the NK cell-mediated cytotoxicity pathway (eFig.8).

3.5 Cytotoxic $CD8^+T$ Cell-Mediated Killing of B Cells and Enhanced Interactions in NMDAR-E Patients

We isolated $CD8^+T$ cells and $CD19^+B$ cells from PBMC of both NMDAR-E patients and control individuals. These cells were then co-cultured in vitro. Live-cell imaging revealed direct contact between $CD8^+T$ cells and B cells, leading to the killing of B cells by $CD8^+T$ cells (Fig.6A). Flow cytometric analysis demonstrated a significant increase in the apoptosis rate of B cells and B cell subclusters in NMDAR-E patients compared to the control individuals (Fig.6B, Fig.6C, and eFig.9). These results suggest that cytotoxic $CD8^+T$ cells may play a role in regulating the immune homeostasis in NMDAR-E patients by eliminating B cells.

Furthermore, the analysis of cell interaction revealed a stronger interaction between KIR^+CD8^+T cells and both naïve and memory B cell subpopulations in both CSF and PB samples of NMDAR-E patients compared to the control group (Fig.6D). Receptor-ligand pairing analysis identified specific interactions between the KIRs expressed by KIR^+CD8^+T cells (including *KIR3DL1*, *KIR2DL3*, and *KIR2DL1)* in the CSF and PB of NMDAR-E patients, as well as NK-related molecules (*KLRC2* and *KLRK1*), with MHC class I molecules expressed on B cells (including HLA-A, HLA-C, and HLA-E) (Fig.6E).

4. Discussion

There have been extensive studies on the roles of B cells and autoantibodies in anti-NMDAR receptor encephalitis. However, while there is increasing evidence suggesting the involvement of T cells in this disease, the contribution of T cell subsets in NMDAR-E patients remains unclear. This study used scRNA-seq, scTCR-seq, and flow cytometry analysis to investigate the phenotypes and potential roles of T cell subsets in NMDAR-E patients. Our study found the activation and TCR clonality of $CD8^+T$ cells in both the CSF and PB of NMDAR-E patients. Additionally, we observed an elevated presence of KIR^+CD8^+T cells in the CSF and PB of NMDAR-E patients. Moreover, through in vitro co-culturing of $CD8^+T$ cells and B cells, we discovered a higher apoptosis rate of B cells in the PB of NMDAR-E patients compared to the control group. These findings offer novel perspectives on the involvement of cytotoxic $CD8^+T$ cells in the pathogenesis of anti-NMDAR receptor encephalitis.

Through the integration of scRNA-seq and flow cytometry analysis, we have discovered a notable rise in the abundance of $CD45RA^+$effector memory $CD8^+T$ cells in both the CSF and PB of NMDAR-E patients. Additionally, in an NMDAR-E mouse model, a significant increase in the number of $CD8^+T$ cells was observed at the 6th

week of modeling, suggesting potential infiltration of $CD8^+$T cells into the brain tissue of the model mice [19]. However, several case studies reported a relatively low number of cytotoxic T cells in the brain tissue of NMDAR-E patients during postmortem or biopsy examinations[16-18]. This observation implies that cytotoxic T cells may not be a primary characteristic of human NMDAR-E disease. Nevertheless, these findings should be interpreted cautiously, considering factors such as the limited number of clinical cases, disease progression, and variations in sampling sites. Our study has been strengthened by increasing the sample size and employing a combination of various methods, which has improved the reliability of our findings. However, given the challenges associated with acquiring brain tissue samples from NMDAR-E patients, it may be necessary to conduct further research using mouse models to explore the influence of specific $CD8^+$T cell subpopulations on NMDAR-E brain tissue.

Upon recognizing cognate antigens, $CD8^+$T cells undergo rapid clonal expansion and differentiation into effector and memory cells [35]. TCR expansion has been reported in several CNS disorder, including multiple sclerosis [36], Parkinson's disease [37], and Alzheimer's disease [30]. Our study found highly clonal T cells in the CSF and PB of NMDAR-E encephalitis patients, mainly composed of effector $CD8^+$T cells. DEGs analysis suggested that autoimmune T cell activity may have potential cytotoxic and chemotactic characteristics. In addition, self-reactive cytotoxic T cells were found to recognize self-antigens in findings on Alzheimer's disease [30], leading to target cell death and exacerbating neuroinflammation. Hence, investigating the role of self-reactive $CD8^+$T cells in CNS diseases holds immense significance and warrants further exploration in the future. For instance, searching for specific TCR sequences that recognize NMDA self-antigens can help better understand the pathogenesis of NMDAR-E encephalitis and provide a basis for the development of more accurate diagnostic and therapeutic methods.

Although the majority of $CD8^+$T cells are traditionally believed to be involved in controlling infections caused by pathogens or targeting cancer cells, emerging evidence indicates the presence of a distinct subset of $CD8^+$T cells that modulate the self-immune response[38]. The regulatory role of $CD8^+$T cells in the immune response was initially observed in the mouse model of experimental autoimmune encephalomyelitis (EAE) by researchers [39, 40]. In 2019, Saligrama et al. reported that $CD8^+$T cells possess the ability to suppress self-reactive $CD4^+$T cells [34]. Furthermore, in 2022, Li et al. discovered a distinct subset of regulatory KIR^+CD8^+T cells that selectively suppress pathogenic $CD4^+$T cells in autoimmune diseases [33]. The regulatory function of KIR^+ $CD8^+$T cells is dependent on the recognition of both classical [34] and non-classical MHC-I molecules expressed on target cells[41-43]. It is important to note that the inhibitory function of KIR^+CD8^+T cells requires the activation of the TCR for full effectiveness [33]. Consistent with previous studies[34, 41-43], our research demonstrates that KIR^+CD8^+T cells enhance their interactions with B cells, as indicated by cell communication analysis. These interactions are facilitated through the expression of MHC-I antigen presentation molecules on B cells.

Moreover, our in vitro co-culture experiments revealed that $CD8^+$T cells obtained from NMDAR-E patients can directly engage and eliminate autologous B cells. Flow cytometry analysis demonstrated a higher rate of apoptosis in B cells derived from NMDAR-E patients compared to control samples. Hence, these findings suggest that in anti-NMDAR encephalitis, certain activated and differentiated effector $CD8^+$T cell subsets, such as the inhibitory KIR^+CD8^+T cells, may modulate the self-immune response by establishing contact with B cells via MHC-I antigen presentation molecules, thereby inducing B cell apoptosis. Further investigations are necessary to verify whether this population of inhibitory $CD8^+$T cells indeed corresponds to KIR^+CD8^+T cells.

There are several limitations in our study. Firstly, our sample size used for scRNA-Seq analysis was relatively limited. However, to mitigate this limitation, we expanded our study by performing flow cytometry analysis on a more extensive range of T cell subpopulations derived from both NMDAR-E patients and control subjects. This augmentation in sample size significantly enhanced the robustness of our findings and bolstered the reliability of our conclusions. Secondly, we utilized publicly available databases as controls for the CSF, which may introduce potential batch effects. However, to minimize the impact of batch effects as much as possible, we employed the scVI method for data analysis, ensuring the reliability and validity of our results. Lastly, it is worth noting that our study solely relied on samples obtained from NMDAR-E patients, which provided a direct reflection of the disease state. However, the study's depth was constrained by the challenges associated with acquiring tissue samples. Consequently, to gain a more profound comprehension of the underlying mechanisms behind these phenotypes, future investigations should incorporate more extensive mechanistic studies utilizing animal models. By adopting such research designs, we can delve deeper into the mechanisms involved and achieve a more comprehensive understanding of the underlying processes.

In conclusion, our study suggests the potential involvement of $CD8^+$T cells in the pathological processes of this disease and highlight their potential therapeutic value in exploring new treatment approaches in the future.

Acknowledgment

The authors express their gratitude to Genenergy Shanghai for their support, as well as to all the patients who generously participated in the study.

Study Founding

This work was supported by grants from National Science Foundation of China (Grant No. 81571272 and 82071459); The 1.3.5 project for disciplines of excellence and Brain Science project of West China Hospital, Sichuan University (Grant No: ZYGD20011 and ZYJC21001).

Author contributions

Jinmei Li and Dong Zhou designed this study and revised the final version of the draft. Sisi Li and Xiang Hu carried out this study; those authors collected samples, analyzed data, wrote the draft, and contributed equally to this study; Yi Yang, Jierui Wang, and Zihua He, and Luoting Yu assisted in collecting the samples; Zhen Hong edited the manuscript.

Declarations of interest

The authors declare no disclosures relevant to the manuscript.

Data availability statement

The raw sequence data reported in this article are currently being uploaded to the Genome Sequence Archive (GSA: PRJCA014916) at the National Genomics Data Center, Beijing Institute of Genomics, Chinese Academy of Sciences. Once the upload is complete, these data will be publicly accessible at https://ngdc.cncb.ac.cn/gsa. Currently, interested parties can request access to the relevant data by contacting the corresponding author. The data sets supporting the conclusions of this article are included within the article and its accompanying files.

References

[1] F. Graus, M.J. Titulaer, R. Balu, S. Benseler, C.G. Bien, T. Cellucci, I. Cortese, R.C. Dale, J.M. Gelfand, M. Geschwind, C.A. Glaser, J. Honnorat, R. Höftberger, T. Iizuka, S.R. Irani, E. Lancaster, F. Leypoldt, H. Prüss, A. Rae-Grant, M. Reindl, M.R. Rosenfeld, K. Rostásy, A. Saiz, A. Venkatesan, A. Vincent, K.P. Wandinger, P. Waters, J. Dalmau, A clinical approach to diagnosis of autoimmune encephalitis, The Lancet. Neurology, 15 (2016) 391-404.

[2] A.J. Gleichman, L.A. Spruce, J. Dalmau, S.H. Seeholzer, D.R. Lynch, Anti-NMDA receptor encephalitis antibody binding is dependent on amino acid identity of a small region within the GluN1 amino terminal domain, J Neurosci, 32 (2012) 11082-11094.

[3] J. Dalmau, E. Lancaster, E. Martinez-Hernandez, M.R. Rosenfeld, R. Balice-Gordon, Clinical experience and laboratory investigations in patients with anti-NMDAR encephalitis, The Lancet. Neurology, 10 (2011) 63-74.

[4] J. Dalmau, T. Armangué, J. Planagumà, M. Radosevic, F. Mannara, F. Leypoldt, C. Geis, E. Lancaster, M.J. Titulaer, M.R. Rosenfeld, F. Graus, An update on anti-NMDA receptor encephalitis for neurologists and psychiatrists: mechanisms and models, The Lancet Neurology, 18 (2019) 1045-1057.

[5] M.J. Titulaer, L. McCracken, I. Gabilondo, T. Armangué, C. Glaser, T. Iizuka, L.S. Honig, S.M. Benseler, I. Kawachi, E. Martinez-Hernandez, E. Aguilar, N. Gresa-Arribas, N. Ryan-Florance, A. Torrents, A. Saiz, M.R. Rosenfeld, R. Balice-Gordon, F. Graus, J. Dalmau, Treatment and prognostic factors for long-term outcome in patients with anti-NMDA receptor encephalitis: an observational cohort study, The Lancet Neurology, 12 (2013) 157-165.

[6] X. Xu, Q. Lu, Y. Huang, S. Fan, L. Zhou, J. Yuan, X. Yang, H. Ren, D. Sun, Y. Dai, H. Zhu, Y. Jiang, Y. Zhu, B. Peng, L. Cui, H. Guan, Anti-NMDAR encephalitis: A single-center, longitudinal study in China, Neurol Neuroimmunol Neuroinflamm, 7 (2020).

[7] M.S. Gable, H. Sheriff, J. Dalmau, D.H. Tilley, C.A. Glaser, The frequency of autoimmune N-methyl-D-aspartate receptor encephalitis surpasses that of individual viral etiologies in young individuals enrolled in the California Encephalitis Project, Clin Infect Dis, 54 (2012) 899-904.

[8] H. Prüss, J. Dalmau, L. Harms, M. Höltje, G. Ahnert-Hilger, K. Borowski, W. Stoecker, K.P. Wandinger, Retrospective analysis of NMDA receptor antibodies in encephalitis of unknown origin, Neurology, 75 (2010) 1735-1739.

[9] J. Heine, U.A. Kopp, J. Klag, C.J. Ploner, H. Prüss, C. Finke, Long-Term Cognitive Outcome in Anti-N-Methyl-D-Aspartate Receptor Encephalitis, Ann Neurol, 90 (2021) 949-961.

[10] E. Tüzün, L. Zhou, J.M. Baehring, S. Bannykh, M.R. Rosenfeld, J. Dalmau, Evidence for antibody-mediated pathogenesis in anti-NMDAR encephalitis associated with ovarian teratoma, Acta neuropathologica, 118 (2009) 737-743.

[11] J. Kreye, N.K. Wenke, M. Chayka, J. Leubner, R. Murugan, N. Maier, B. Jurek, L.T. Ly, D. Brandl, B.R. Rost, A. Stumpf, P. Schulz, H. Radbruch, A.E. Hauser, F. Pache, A. Meisel, L. Harms, F. Paul, U. Dirnagl, C. Garner, D. Schmitz, H. Wardemann, H. Pruss, Human cerebrospinal fluid monoclonal N-methyl-D-aspartate receptor autoantibodies are sufficient for encephalitis pathogenesis, Brain, 139 (2016) 2641-2652.

[12] N.K. Wenke, J. Kreye, E. Andrzejak, A. van Casteren, J. Leubner, M.S. Murgueitio, S.M. Reincke, C. Secker, L. Schmidl, C. Geis, F. Ackermann, M. Nikolaus, C.C. Garner, H. Wardemann, G. Wolber, H. Pruss, N-methyl-D-aspartate receptor dysfunction by unmutated human antibodies against the NR1 subunit, Ann Neurol, 85 (2019) 771-776.

[13] J.I. Byun, S.T. Lee, J. Moon, K.H. Jung, J.S. Sunwoo, J.A. Lim, T.J. Kim, Y.W. Shin, K.J. Lee, J.S. Jun, H.S. Lee, W.J. Lee, Y.S. Kim, S. Kim, D. Jeon, K.I. Park, K.Y. Jung, M. Kim, K. Chu, S.K. Lee, Distinct intrathecal interleukin-17/interleukin-6 activation in anti-N-methyl-d-aspartate receptor encephalitis, J Neuroimmunol, 297 (2016) 141-147.

[14] Z. Liba, J. Kayserova, M. Elisak, P. Marusic, H. Nohejlova, J. Hanzalova, V. Komarek, A. Sediva, Anti-N-methyl-D-aspartate receptor encephalitis: the clinical course in light of the chemokine and cytokine levels in cerebrospinal fluid, J Neuroinflammation, 13 (2016) 55.

[15] J. Liu, L. Liu, W. Kang, G. Peng, D. Yu, Q. Ma, Y. Li, Y. Zhao, L. Li, F. Dai, J. Wang, Cytokines/Chemokines: Potential Biomarkers for Non-paraneoplastic Anti-N-Methyl-D-Aspartate Receptor Encephalitis, Front Neurol, 11 (2020) 582296.

[16] J.P. Camdessanche, N. Streichenberger, G. Cavillon, V. Rogemond, G. Jousserand, J. Honnorat, P. Convers, J.C. Antoine, Brain immunohistopathological study in a patient with anti-NMDAR encephalitis, Eur J Neurol, 18 (2011) 929-931.

[17] C.G. Bien, A. Vincent, M.H. Barnett, A.J. Becker, I. Blümcke, F. Graus, K.A. Jellinger, D.E. Reuss, T. Ribalta, J. Schlegel, I. Sutton, H. Lassmann, J. Bauer, Immunopathology of autoantibody-associated encephalitides: clues for pathogenesis, Brain, 135 (2012) 1622-1638.

[18] E. Martinez-Hernandez, J. Horvath, Y. Shiloh-Malawsky, N. Sangha, M. Martinez-Lage, J. Dalmau, Analysis of complement and plasma cells in the brain of patients with anti-NMDAR encephalitis, Neurology, 77 (2011) 589-593.

[19] B.E. Jones, K.R. Tovar, A. Goehring, F. Jalali-Yazdi, N.J. Okada, E. Gouaux, G.L. Westbrook, Autoimmune receptor encephalitis in mice induced by active immunization with conformationally stabilized holoreceptors, Sci Transl Med, 11 (2019).

[20] Y. Shu, F. Peng, B. Zhao, C. Liu, Q. Li, H. Li, Y. Wang, Y. Jiang, T. Lu, Q. Wang, J. Sun, H. Feng, Z. Lu, X. Liu, J. Wang, W. Qiu, Transfer of patient's peripheral blood mononuclear cells (PBMCs) disrupts blood-brain barrier and induces anti-NMDAR encephalitis: a study of novel humanized PBMC mouse model, J Neuroinflammation, 20 (2023) 164.

[21] R. Balu, L. McCracken, E. Lancaster, F. Graus, J. Dalmau, M.J. Titulaer, A score that predicts 1-

year functional status in patients with anti-NMDA receptor encephalitis, Neurology, 92 (2019) e244-e252.
[22] S. Macher, T. Zrzavy, R. Hoftberger, P. Altmann, E. Pataraia, F. Zimprich, T. Berger, P. Rommer, Longitudinal measurement of cerebrospinal fluid neurofilament light in anti-N-methyl-D-aspartate receptor encephalitis, Eur J Neurol, 28 (2021) 1401-1405.
[23] R. Lopez, J. Regier, M.B. Cole, M.I. Jordan, N. Yosef, Deep generative modeling for single-cell transcriptomics, Nat Methods, 15 (2018) 1053-1058.
[24] D. Schafflick, C.A. Xu, M. Hartlehnert, M. Cole, A. Schulte-Mecklenbeck, T. Lautwein, J. Wolbert, M. Heming, S.G. Meuth, T. Kuhlmann, C.C. Gross, H. Wiendl, N. Yosef, G. Meyer Zu Horste, Integrated single cell analysis of blood and cerebrospinal fluid leukocytes in multiple sclerosis, Nat Commun, 11 (2020) 247.
[25] K.R. Moon, D. van Dijk, Z. Wang, S. Gigante, D.B. Burkhardt, W.S. Chen, K. Yim, A.V.D. Elzen, M.J. Hirn, R.R. Coifman, N.B. Ivanova, G. Wolf, S. Krishnaswamy, Visualizing structure and transitions in high-dimensional biological data, Nature biotechnology, 37 (2019) 1482-1492.
[26] S. Jin, C.F. Guerrero-Juarez, L. Zhang, I. Chang, R. Ramos, C.H. Kuan, P. Myung, M.V. Plikus, Q. Nie, Inference and analysis of cell-cell communication using CellChat, Nat Commun, 12 (2021) 1088.
[27] A.M. Luoma, S. Suo, H.L. Williams, T. Sharova, K. Sullivan, M. Manos, P. Bowling, F.S. Hodi, O. Rahma, R.J. Sullivan, G.M. Boland, J.A. Nowak, S.K. Dougan, M. Dougan, G.C. Yuan, K.W. Wucherpfennig, Molecular Pathways of Colon Inflammation Induced by Cancer Immunotherapy, Cell, 182 (2020) 655-671.e622.
[28] A.M. Luoma, S. Suo, Y. Wang, L. Gunasti, C.B.M. Porter, N. Nabilsi, J. Tadros, A.P. Ferretti, S. Liao, C. Gurer, Y.-H. Chen, S. Criscitiello, C.A. Ricker, D. Dionne, O. Rozenblatt-Rosen, R. Uppaluri, R.I. Haddad, O. Ashenberg, A. Regev, E.M. Van Allen, G. MacBeath, J.D. Schoenfeld, K.W. Wucherpfennig, Tissue-resident memory and circulating T cells are early responders to pre-surgical cancer immunotherapy, Cell, (2022).
[29] J.L. Pappalardo, L. Zhang, M.K. Pecsok, K. Perlman, C. Zografou, K. Raddassi, A. Abulaban, S. Krishnaswamy, J. Antel, D. van Dijk, D.A. Hafler, Transcriptomic and clonal characterization of T cells in the human central nervous system, Sci Immunol, 5 (2020).
[30] D. Gate, N. Saligrama, O. Leventhal, A.C. Yang, M.S. Unger, J. Middeldorp, K. Chen, B. Lehallier, D. Channappa, M.B. De Los Santos, A. McBride, J. Pluvinage, F. Elahi, G.K.-Y. Tam, Y. Kim, M. Greicius, A.D. Wagner, L. Aigner, D.R. Galasko, M.M. Davis, T. Wyss-Coray, Clonally expanded CD8 T cells patrol the cerebrospinal fluid in Alzheimer's disease, Nature, 577 (2020) 399-404.
[31] E.H. Wilson, W. Weninger, C.A. Hunter, Trafficking of immune cells in the central nervous system, J Clin Invest, 120 (2010) 1368-1379.
[32] F. Sallusto, D. Lenig, R. Förster, M. Lipp, A. Lanzavecchia, Two subsets of memory T lymphocytes with distinct homing potentials and effector functions, Nature, 401 (1999) 708-712.
[33] J. Li, M. Zaslavsky, Y. Su, J. Guo, M.J. Sikora, V. van Unen, A. Christophersen, S.H. Chiou, L. Chen, J. Li, X. Ji, J. Wilhelmy, A.M. McSween, B.A. Palanski, V.V.A. Mallajosyula, N.A. Bracey, G.K.R. Dhondalay, K. Bhamidipati, J. Pai, L.B. Kipp, J.E. Dunn, S.L. Hauser, J.R. Oksenberg, A.T. Satpathy, W.H. Robinson, C.L. Dekker, L.M. Steinmetz, C. Khosla, P.J. Utz, L.M. Sollid, Y.H. Chien, J.R. Heath, N.Q. Fernandez-Becker, K.C. Nadeau, N. Saligrama, M.M. Davis, KIR(+)CD8(+) T cells suppress pathogenic T cells and are active in autoimmune diseases and COVID-19, Science, 376 (2022) eabi9591.
[34] N. Saligrama, F. Zhao, M.J. Sikora, W.S. Serratelli, R.A. Fernandes, D.M. Louis, W. Yao, X. Ji, J.

Idoyaga, V.B. Mahajan, L.M. Steinmetz, Y.H. Chien, S.L. Hauser, J.R. Oksenberg, K.C. Garcia, M.M. Davis, Opposing T cell responses in experimental autoimmune encephalomyelitis, Nature, 572 (2019) 481-487.
[35] M. Philip, A. Schietinger, CD8(+) T cell differentiation and dysfunction in cancer, Nat Rev Immunol, (2021).
[36] A. Junker, J. Ivanidze, J. Malotka, I. Eiglmeier, H. Lassmann, H. Wekerle, E. Meinl, R. Hohlfeld, K. Dornmair, Multiple sclerosis: T-cell receptor expression in distinct brain regions, Brain, 130 (2007) 2789-2799.
[37] P. Wang, L. Yao, M. Luo, W. Zhou, X. Jin, Z. Xu, S. Yan, Y. Li, C. Xu, R. Cheng, Y. Huang, X. Lin, K. Ma, H. Cao, H. Liu, G. Xue, F. Han, H. Nie, Q. Jiang, Single-cell transcriptome and TCR profiling reveal activated and expanded T cell populations in Parkinson's disease, Cell Discov, 7 (2021) 52.
[38] H. Nakagawa, L. Wang, H. Cantor, H.J. Kim, New Insights Into the Biology of CD8 Regulatory T Cells, Adv Immunol, 140 (2018) 1-20.
[39] D.R. Koh, W.P. Fung-Leung, A. Ho, D. Gray, H. Acha-Orbea, T.W. Mak, Less mortality but more relapses in experimental allergic encephalomyelitis in CD8-/- mice, Science, 256 (1992) 1210-1213.
[40] H. Jiang, S.I. Zhang, B. Pernis, Role of CD8+ T cells in murine experimental allergic encephalomyelitis, Science, 256 (1992) 1213-1215.
[41] H.J. Kim, B. Verbinnen, X. Tang, L. Lu, H. Cantor, Inhibition of follicular T-helper cells by CD8(+) regulatory T cells is essential for self tolerance, Nature, 467 (2010) 328-332.
[42] H.J. Kim, X. Wang, S. Radfar, T.J. Sproule, D.C. Roopenian, H. Cantor, CD8+ T regulatory cells express the Ly49 Class I MHC receptor and are defective in autoimmune prone B6-Yaa mice, Proc Natl Acad Sci U S A, 108 (2011) 2010-2015.
[43] H. Sheng, I. Marrero, I. Maricic, S.S. Fanchiang, S. Zhang, D.B. Sant'Angelo, V. Kumar, Distinct PLZF(+)CD8αα(+) Unconventional T Cells Enriched in Liver Use a Cytotoxic Mechanism to Limit Autoimmunity, J Immunol, 203 (2019) 2150-2162.

Figure legend

Figure 1. Single-cell transcriptomics analysis the T cell composition of CSF and PB.
(A) Schematic representation of the study design (see Methods for details). (B) The t-SNE plot displays 10 distinct clusters of cells, each color-coded and identified based on merged single-cell transcriptomes obtained from blood (NMDAR-E, n=4; HC, n=2) and CSF (NMDAR-E, n=3; IIH, n=6) samples. The assigned cluster names are denoted manually. (C) Expression of marker genes in peripheral T and NK cells was used to classify subclusters. The dot size indicates the percentage of cells expressing the gene, while color represents the average gene expression level per cell. (D-F) These volcano plots illustrate the comparison of CSF and PB cell subpopulations between NMDAR-E patients and controls, as well as the differences in CSF and PB cell subpopulations among NMDAR-E patients. The plots are generated using a beta-binomial regression model and are presented as a fold change (log10) against p value (-log10). The horizontal line denotes the significance threshold. Annotation: CSF, cerebrospinal fluid; PB, periphery blood; gdT, γδ T cells; Tn, naive T cells; Te, effector T cells; Tcm, central memory T cells; Tem, effector memory T cells; Tregs, regulatory $CD4^{+}$T cells; NK, natural killer cells.

Figure 2. Transcriptomic characteristics of T cell subsets in the CSF of patients with anti-NMDAR encephalitis (A-B) Representative contour plots (A) and summary scatter plots (B) show the percentage of $CD45RA^{+}CCR7^{-}$ ($CD8^{+}$Temra), $CD45RA^{+}CCR7^{+}$ ($CD8^{+}$Tn), $CD45RA^{-}CCR7^{+}$ ($CD8^{+}$Tcm), and $CD45RA^{-}CCR7^{-}$ ($CD8^{+}$Tem) cells in CSF from control individuals (n = 12) and NMDAR-E patients (n = 15). **p < 0.01, two-tailed unpaired Student's t test. (C-D) Representative contour plots (C) and summary scatter plots (D) show the percentage of $CD45RA^{+}CCR7^{-}$ ($CD4^{+}$Temra), $CD45RA^{+}CCR7^{+}$ ($CD4^{+}$Tn), $CD45RA^{-}CCR7^{+}$ ($CD4^{+}$Tcm), and $CD45RA^{-}CCR7^{-}$ ($CD4^{+}$Tem) cells in CSF from control individuals (n = 12) and NMDAR-E patients (n = 15). **p < 0.01, two-tailed unpaired Student's t test. Flow charts of for (A-D) are provided in Figure e-3. (E) DEGs within T cell subclusters in the CSF of both NMDAR-E patients and control individuals, and calculated the averaged scaled expression levels across all cells within each group. (F) A bubble plot is presented, depicting enriched terms selected from the upregulated KEGG pathways in the T cell subcluster of CSF samples from NMDAR-E patients compared to control individuals, as identified by comparing matched clusters. The dot size represents the percentage of cells expressing the gene, while the color indicates the average per cell gene expression level. Annotation: CSF, cerebrospinal fluid; DEGs, Differentially expressed genes; gdT, γδ T cells; Tn, naive T cells; Te, effector T cells; Tcm, central memory T cells; Tem, effector memory T cells; Tregs, regulatory $CD4^{+}$T cells; Temra, $CD45RA^{+}$ effector memory T.

Figure 3. Periphery $CD8^{+}$T cells paly a cytotoxic characteristic in patients with anti-NMDAR encephalitis. (A-B) Representative contour plots (A) and summary scatter plots (B) show the percentage of $CD45RA^{+}CCR7^{-}$($CD8^{+}$Temra), $CD45RA^{+}CCR7^{+}$($CD8^{+}$Tn), $CD45RA^{-}CCR7^{+}$ ($CD8^{+}$Tcm), and $CD45RA^{-}CCR7^{-}$ ($CD8^{+}$Tem) cells in PB from control individuals (n =21) and NMDAR-E patients (n = 34). *p < 0.05, **p < 0.01, ***p < 0.001, two-tailed unpaired Student's t test. (C-D) Representative contour plots (A) and summary scatter plots (B) show the percentage of $CD45RA^{+}CCR7^{-}$($CD4^{+}$Temra), $CD45RA^{+}CCR7^{+}$($CD4^{+}$Tn), $CD45RA^{-}CCR7^{+}$($CD4^{+}$Tcm), and $CD45RA^{-}CCR7^{-}$($CD4^{+}$Tem) cells in blood from control individuals (n=21) and NMDAR-E patients (n = 34). Flow charts of for (A-D) are provided in Figure e-3. (E) Identification of DEGs among T cell subclusters in the blood of NMDAR-E patients and control individuals, with calculation of the averaged scaled expression levels across all cells within each group. (F-G) Violin plots showing selected DEGs associated with cytotoxicity (F) and promoting T cell entry into the central nervous system (G), with normalized transcript counts displayed on the y-axis. (H) A bubble plot that displays the enriched terms selected from the T cell subcluster in the blood of NMDAR-E patients compared to control individuals. (I-J) Flow cytometry plots (I) and corresponding scatter plots (J) presenting the frequency of $CD8^{+}$T cell subsets in the peripheral blood of NMDAR-E patients with mild/moderate severity (n = 13) and severe disease (n = 21). (K-L) Flow cytometry plots (K) and corresponding scatter plots (L) demonstrating the frequency of $CD8^{+}$T cell subsets in the blood of healthy controls (n = 21), acute-stage NMDAR-E patients (n = 34), and relapsed NMDAR-E patients (n = 13). *p < 0.05, **p < 0.01, ***P< 0.001, two-tailed unpaired Student's t test. Annotation: CSF, cerebrospinal fluid; DEGs, differentially expressed genes; gdT, γδ T cells; Tn, naive T cells; Te, effector T cells; Tcm, central memory T cells; Tem, effector memory T cells; Tregs, regulatory $CD4^{+}$T cells; Temra, $CD45RA^{+}$ effector memory T.

Figure 4. Significant TCR clone expansion of CD8$^+$T cells in both CSF and PB of NMDAR-E patients. (A) Distribution of clonal cells in T cell clusters found in the CSF of NMDAR-E patients (n=3), blood of NMDAR-E patients (n=4), and healthy controls (n=2). (B) TCRαβ clonality of T cells in CSF and blood samples from NMDAR-E patients, as well as blood samples from healthy controls, represented with clones color-coded according to their proportion of total TCRαβ sequences. (C-E) Bar graphs illustrating the cellular proportions of three different clonal expansion groups in each T cell cluster, derived from blood samples of healthy controls (C), blood samples of NMDAR-E patients (D), and CSF samples of NMDAR-E patients (E). (F-G) Volcano plots comparing the differential gene expression between highly clonal (clonal TCRαβ $\geq$ 3) and unclonal T cells in both blood (F) and CSF (G) samples from NMDAR-E patients. Detailed source data for (F, G) are provided in Supplementary Dataset 2. (H) Heatmaps showing selected genes differentially expressed in highly clonal (clonal TCRαβ $\geq$ 3) in blood and CSF of NMDAR-E patients, compared to unclonal T cells. Heatmap colors indicate z-scored values for mean gene expression in each group. (I-J) Sharing of expanded TCR clonotypes across T cell clusters in the blood (I) and CSF (J) of NMDAR-E patients. The bottom heatmap shows the number of shared expanded TCR clonotypes for each cluster pair in NMDAR-E patients.

Figure 5. Changes and transcriptional characteristics of KIR$^+$CD8 T cells in NMDAR-E patients (A) Expression of KIR transcripts (KIR3DL1 and KIR2DL3) in CD8$^+$T cells from the CSF and blood of control individuals (CSF, n= 6; Blood, n=2) and NMDAR-E patients (CSF, n=3; Blood, n=4). (B) t-SNE plots showing the distribution of KIR$^+$CD8$^+$T cells (expressing KIR3DL1, KIR3DL2, KIR2DL1, or KIR2DL3 genes) and KIR$^-$CD8$^+$T cells in the CSF and blood of controls and NMDAR-E patients. (C) The KIR$^+$CD8$^+$T cell population shown in Fig.5B is primarily composed of three subsets: CD8$^+$Tem, CD8$^+$Te, and CD8$^+$Tcm. The proportion of CD8$^+$Tn subset is minimal. (D-E) Representative contour plots (D) and summary scatter plots (E) show the percentage of CD158e$^+$cells in CD8$^+$T cells from the blood of healthy controls (n = 11), NMDAR-E patients with mild/moderate disease (n =10), severe disease (n =9), relapsed NMDAR-E patients (n=13), and patients in remission (n =8). (F-G) Representative contour plots (F) and summary scatter plots (G) show the percentage of CD45RA$^+$cells in CD158e$^+$CD8$^+$T cells (KIR$^+$CD8$^+$Temra) from the blood of healthy controls (n = 11), NMDAR-E patients with mild/moderate disease (n =10), severe disease (n =9), relapsed NMDAR-E patients (n =13), and patients in remission (n =8). Flow charts of for (D-G) are provided in Figure e-7A. (H) t-SNE plots of KIR$^+$ CD8$^+$T cells from NMDAR-E patients and controls with clonal and clonal cells annotated with different colors (clonal, red; unclonal, green). (I) TCRαβ clonality of KIR$^+$CD8$^+$T in the CSF and blood of NMDAR-E patients and blood of healthy control individuals. Clones are colored by proportion of the total TCRαβ sequences. (J) The differential expression of expanded clones revealed increased expression of cytotoxic effector genes in the clonal KIR$^+$CD8$^+$T cells of NMDAR-E patients as compared to unclonal KIR$^+$CD8$^+$T in both blood and CSF samples.

Figure 6. Inhibition of B cells by cytotoxic CD8$^+$T cells in the blood of NMDAR-E patients. (A) The process of interaction between CD8$^+$T cells and B cells from the peripheral blood of NMDAR-E patients was observed through live cell imaging. Specifically, CD8$^+$T cells approached (a), contacted (b), engaged in cytotoxic activity against (c) and eventually detached from B cells (d). The white arrow represents CD19$^+$B cells, while the black arrow represents CD8$^+$T cells. Red

fluorescently labeled apoptotic target cells. Scale bars = 10 um. (B) Representative contour plots and summary scatter plots showing the percentage of $7AAD^{-}$Annexin V^{-} (Q4, surviving cells) and Annexin V^{+} (Q2 and Q3, apoptotic cells) B cells, naïve B cells (Bn), and memory B cells (Bm) in the blood of 7 healthy controls (HCs) and 11 NMDAR-E patients. **P < 0.01; ***P < 0.001; ****P < 0.0001; evaluated using two-tailed unpaired Student's t test. (C) Summary scatter plots showing the percentage of surviving and apoptotic ASCs and DN cells in the blood of 7 healthy controls (HCs) and 11 NMDAR-E patients. **P < 0.01; evaluated using two-tailed unpaired Student's t test. Flow charts of for (B and C) are provided in Figure e-9. (D) Cell-cell interaction analysis predicts interactions between $KIR^{+}CD8^{+}$T cells and $KIR^{-}CD8^{+}$T cells with plasma cells, naïve B (Bn) cells, and memory B (Bm) cells in the CSF and blood of controls and NMDAR-E patients. (E) Dot plot illustrating cell-cell interactions between $KIR^{+}CD8^{+}$T cells and plasma cells, Bn cells, and Bm cells from single-cell RNA-sequencing data, based on selected cytokines and molecules calculated by CellPhoneDB. Annotation: Bn, naïve B cells; Bm, memory B cells ; ASCs, Antibody-secreting cells; DN, CD27-IgD-double negative B cells; AE, autoimmune encephalitis (Refers to anti-NMDAR encephalitis).

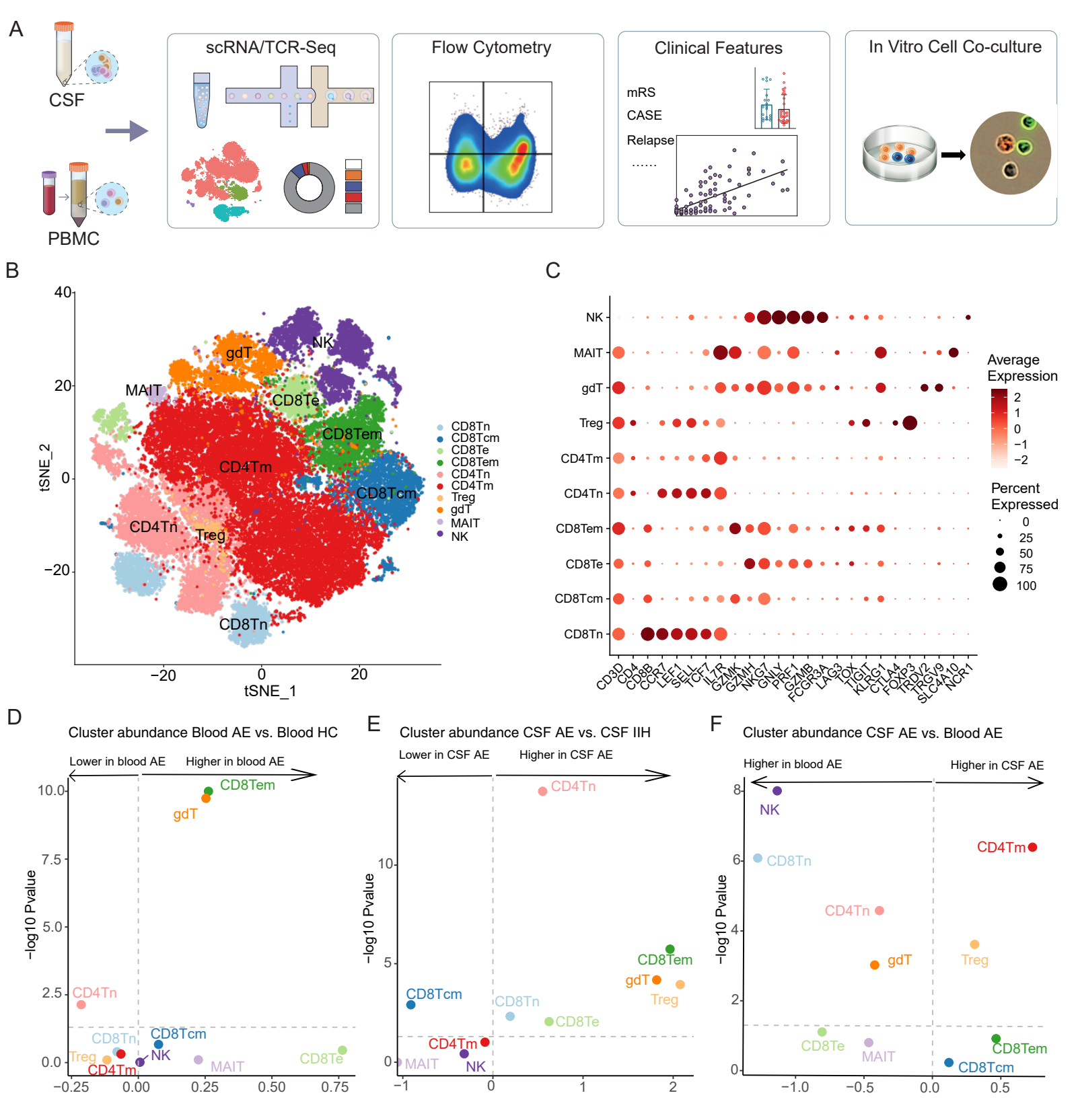
A
CSF
PBMC
scRNA/TCR-Seq
Flow Cytometry
Clinical Features
mRS
CASE
Relapse
.....
In Vitro Cell Co-culture
B
tSNE_2
tSNE_1
gdT
NK
MAIT
CD8Te
CD8Tem
CD4Tm
CD8Tcm
CD4Tn
Treg
CD8Tn
CD8Tn
CD8Tcm
CD8Te
CD8Tem
CD4Tn
CD4Tm
Treg
gdT
MAIT
NK
C
Average Expression
Percent Expressed
CD3D
CD4
CD8B
CCR7
LEF1
SELL
TCF7
IL7R
GZMK
GZMH
NKG7
GNLY
PRF1
GZMB
FCGR3A
LAG3
TOX
TIGIT
KLRG1
CTLA4
FOXP3
TRDV2
TRGV9
SLC4A10
NCR1
D
Cluster abundance Blood AE vs. Blood HC
Lower in blood AE
Higher in blood AE
−log10 Pvalue
E
Cluster abundance CSF AE vs. CSF IIH
Lower in CSF AE
Higher in CSF AE
F
Cluster abundance CSF AE vs. Blood AE
Higher in blood AE
Higher in CSF AE

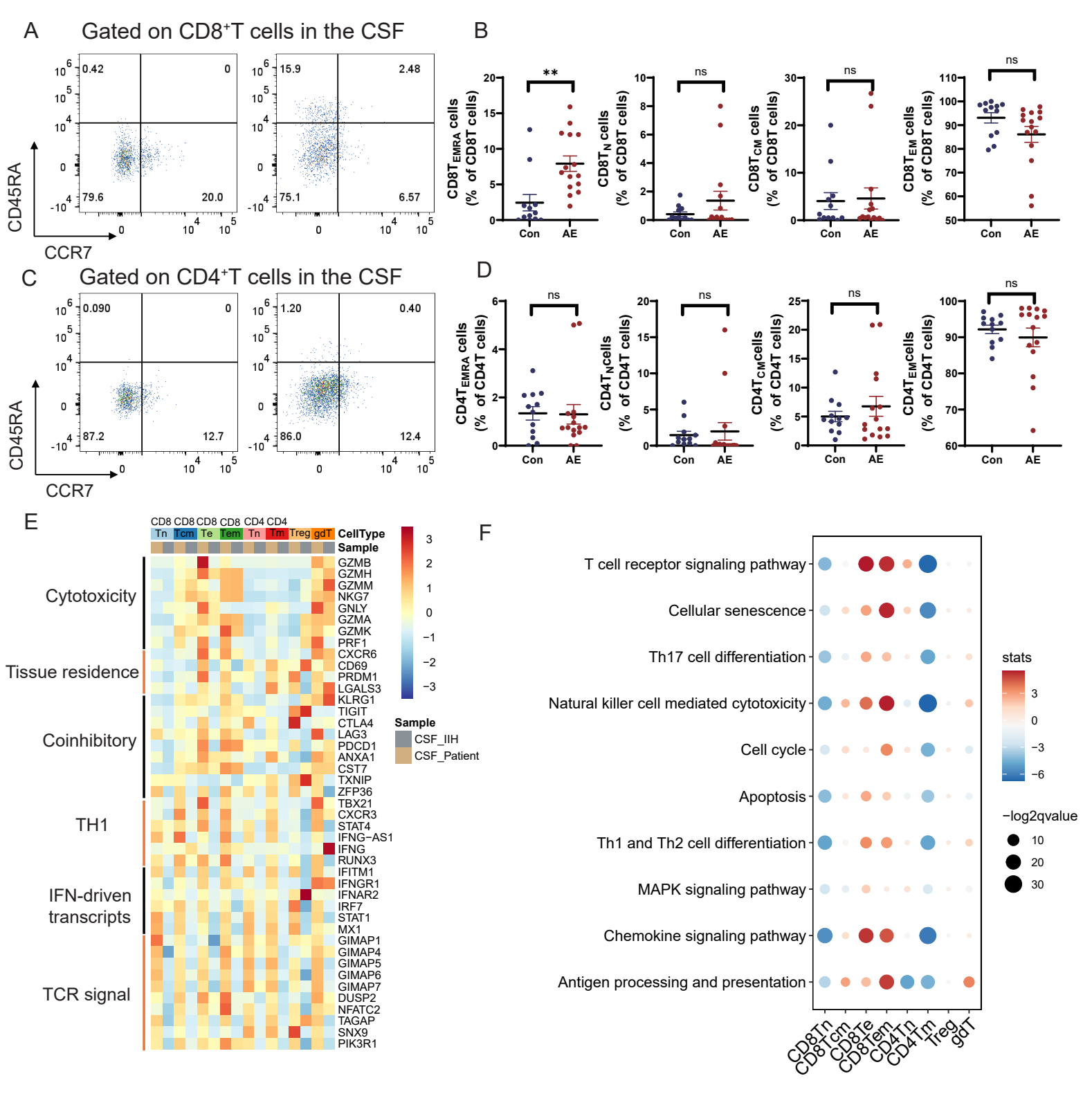
A
Gated on CD8+T cells in the CSF
CD45RA
CCR7
0.42
0
79.6
20.0
15.9
2.48
75.1
6.57
B
CD8TEMRA cells (% of CD8T cells)
CD8TN cells (% of CD8T cells)
CD8TCM cells (% of CD8T cells)
CD8TEM cells (% of CD8T cells)
**
ns
Con
AE
C
Gated on CD4+T cells in the CSF
0.090
1.20
0.40
87.2
12.7
86.0
12.4
D
CD4TEMRA cells (% of CD4T cells)
CD4TNcells (% of CD4T cells)
CD4TCMcells (% of CD4T cells)
CD4TEMcells (% of CD4T cells)
E
CD8 CD8 CD8 CD8 CD4 CD4
Tn Tcm Te Tem Tn Tm Treg gdT
CellType
Sample
Cytotoxicity
Tissue residence
Coinhibitory
TH1
IFN-driven transcripts
TCR signal
GZMB
GZMH
GZMM
NKG7
GNLY
GZMA
GZMK
PRF1
CXCR6
CD69
PRDM1
LGALS3
KLRG1
TIGIT
CTLA4
LAG3
PDCD1
ANXA1
CST7
TXNIP
ZFP36
TBX21
CXCR3
STAT4
IFNG-AS1
IFNG
RUNX3
IFITM1
IFNGR1
IFNAR2
IRF7
STAT1
MX1
GIMAP1
GIMAP4
GIMAP5
GIMAP6
GIMAP7
DUSP2
NFATC2
TAGAP
SNX9
PIK3R1
CSF_IIH
CSF_Patient
F
T cell receptor signaling pathway
Cellular senescence
Th17 cell differentiation
Natural killer cell mediated cytotoxicity
Cell cycle
Apoptosis
Th1 and Th2 cell differentiation
MAPK signaling pathway
Chemokine signaling pathway
Antigen processing and presentation
CD8Tn
CD8Tcm
CD8Te
CD8Tem
CD4Tn
CD4Tm
Treg
gdT
stats
−log2qvalue

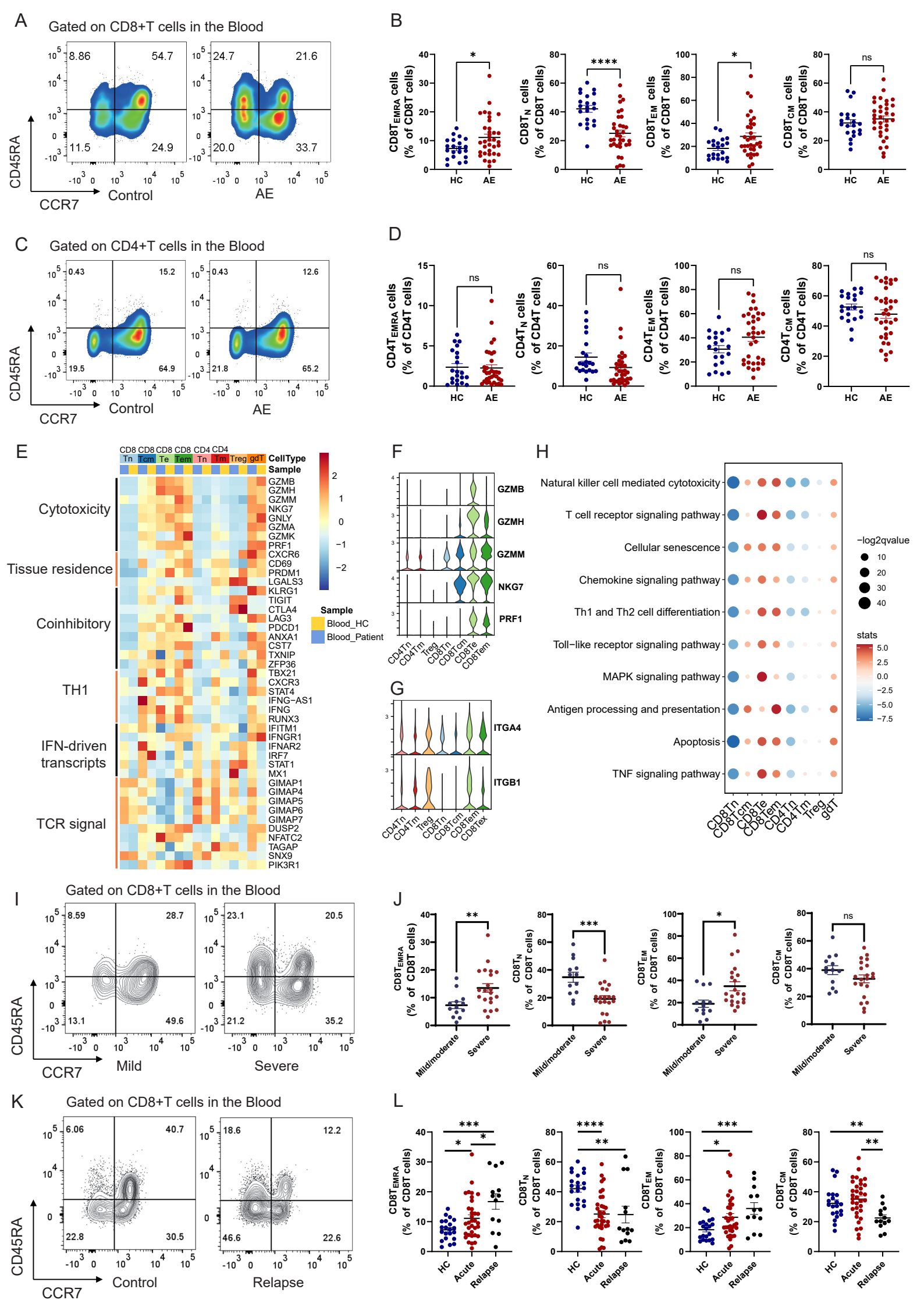
A
Gated on CD8+T cells in the Blood
8.86
54.7
11.5
24.9
24.7
21.6
20.0
33.7
CD45RA
CCR7
Control
AE
B
CD8T_EMRA cells (% of CD8T cells)
CD8T_N cells (% of CD8T cells)
CD8T_EM cells (% of CD8T cells)
CD8T_CM cells (% of CD8T cells)
HC
AE
ns
C
Gated on CD4+T cells in the Blood
0.43
15.2
19.5
64.9
0.43
12.6
21.8
65.2
CD45RA
CCR7
Control
AE
D
CD4T_EMRA cells (% of CD4T cells)
CD4T_N cells (% of CD4T cells)
CD4T_EM cells (% of CD4T cells)
CD4T_CM cells (% of CD4T cells)
HC
AE
ns
E
CD8 CD8 CD8 CD8 CD4 CD4
Tn Tcm Te Tem Tn Tm Treg gdT
CellType
Sample
Cytotoxicity
Tissue residence
Coinhibitory
TH1
IFN-driven transcripts
TCR signal
GZMB
GZMH
GZMM
NKG7
GNLY
GZMA
GZMK
PRF1
CXCR6
CD69
PRDM1
LGALS3
KLRG1
TIGIT
CTLA4
LAG3
PDCD1
ANXA1
CST7
TXNIP
ZFP36
TBX21
CXCR3
STAT4
IFNG-AS1
IFNG
RUNX3
IFITM1
IFNGR1
IFNAR2
IRF7
STAT1
MX1
GIMAP1
GIMAP4
GIMAP5
GIMAP6
GIMAP7
DUSP2
NFATC2
TAGAP
SNX9
PIK3R1
Sample
Blood_HC
Blood_Patient
F
GZMB
GZMH
GZMM
NKG7
PRF1
CD4Tn
CD4Tm
Treg
CD8Tn
CD8Tcm
CD8Te
CD8Tem
G
ITGA4
ITGB1
CD4Tn
CD4Tm
Treg
CD8Tn
CD8Tcm
CD8Tem
CD8Tex
H
Natural killer cell mediated cytotoxicity
T cell receptor signaling pathway
Cellular senescence
Chemokine signaling pathway
Th1 and Th2 cell differentiation
Toll-like receptor signaling pathway
MAPK signaling pathway
Antigen processing and presentation
Apoptosis
TNF signaling pathway
CD8Tn
CD8Tcm
CD8Te
CD8Tem
CD4Tn
CD4Tm
Treg
gdT
-log2qvalue
stats
I
Gated on CD8+T cells in the Blood
8.59
28.7
13.1
49.6
23.1
20.5
21.2
35.2
CD45RA
CCR7
Mild
Severe
J
CD8T_EMRA (% of CD8T cells)
CD8T_N (% of CD8T cells)
CD8T_EM (% of CD8T cells)
CD8T_CM (% of CD8T cells)
Mild/moderate
Severe
ns
K
Gated on CD8+T cells in the Blood
6.06
40.7
22.8
30.5
18.6
12.2
46.6
22.6
CD45RA
CCR7
Control
Relapse
L
CD8T_EMRA (% of CD8T cells)
CD8T_N (% of CD8T cells)
CD8T_EM (% of CD8T cells)
CD8T_CM (% of CD8T cells)
HC
Acute
Relapse

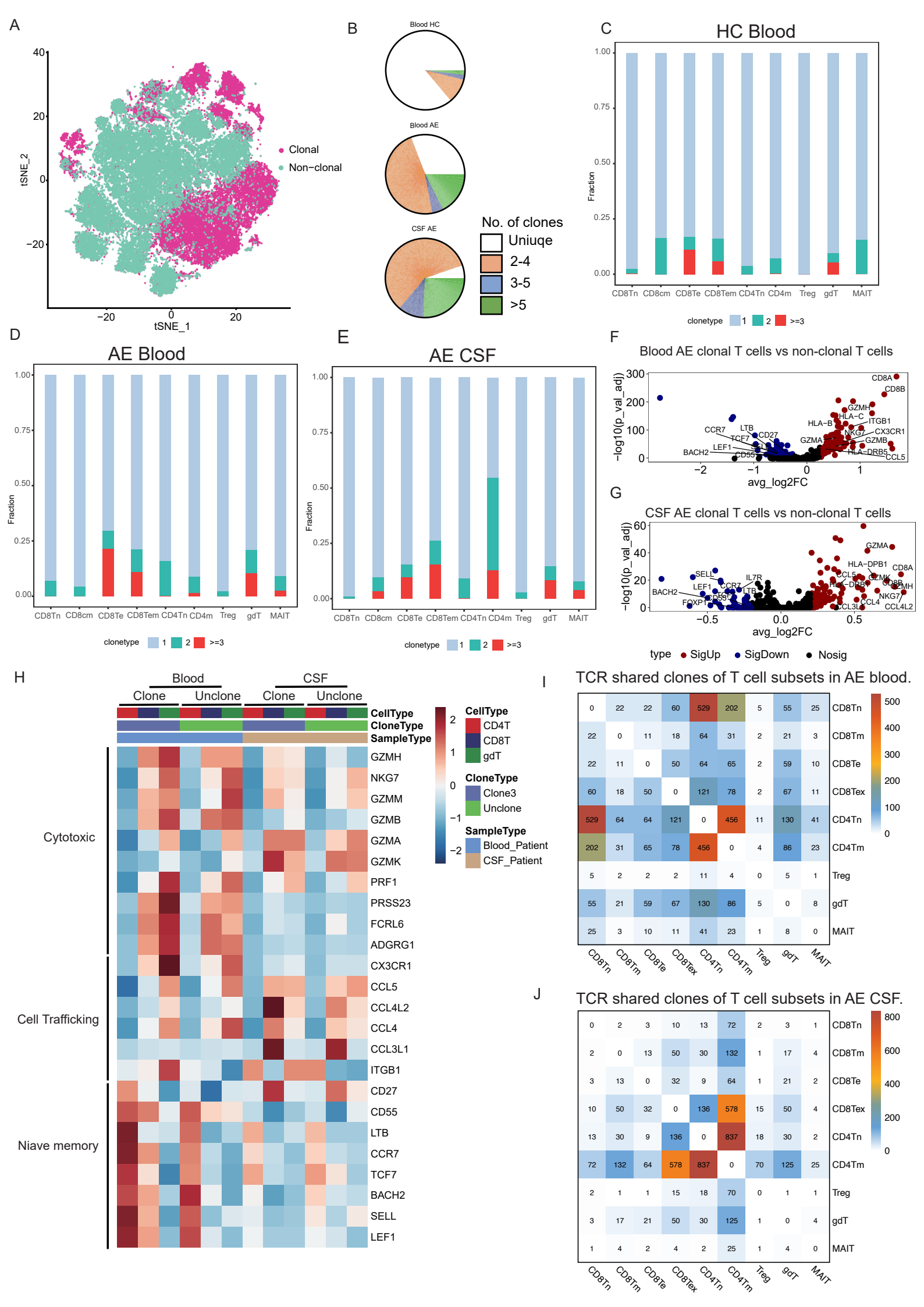
A
tSNE_2
tSNE_1
Clonal
Non−clonal
B
Blood HC
Blood AE
CSF AE
No. of clones
Uniuqe
2-4
3-5
>5
C
HC Blood
Fraction
CD8Tn CD8cm CD8Te CD8Tem CD4Tn CD4m Treg gdT MAIT
clonetype 1 2 >=3
D
AE Blood
Fraction
CD8Tn CD8cm CD8Te CD8Tem CD4Tn CD4m Treg gdT MAIT
clonetype 1 2 >=3
E
AE CSF
Fraction
CD8Tn CD8cm CD8Te CD8Tem CD4Tn CD4m Treg gdT MAIT
clonetype 1 2 >=3
F
Blood AE clonal T cells vs non-clonal T cells
−log10(p_val_adj)
avg_log2FC
G
CSF AE clonal T cells vs non-clonal T cells
−log10(p_val_adj)
avg_log2FC
type SigUp SigDown Nosig
H
Blood
CSF
Clone
Unclone
CellType
CloneType
SampleType
CD4T
CD8T
gdT
Clone3
Unclone
Blood_Patient
CSF_Patient
Cytotoxic
Cell Trafficking
Niave memory
GZMH
NKG7
GZMM
GZMB
GZMA
GZMK
PRF1
PRSS23
FCRL6
ADGRG1
CX3CR1
CCL5
CCL4L2
CCL4
CCL3L1
ITGB1
CD27
CD55
LTB
CCR7
TCF7
BACH2
SELL
LEF1
I
TCR shared clones of T cell subsets in AE blood.
CD8Tn CD8Tm CD8Te CD8Tex CD4Tn CD4Tm Treg gdT MAIT
J
TCR shared clones of T cell subsets in AE CSF.
CD8Tn CD8Tm CD8Te CD8Tex CD4Tn CD4Tm Treg gdT MAIT

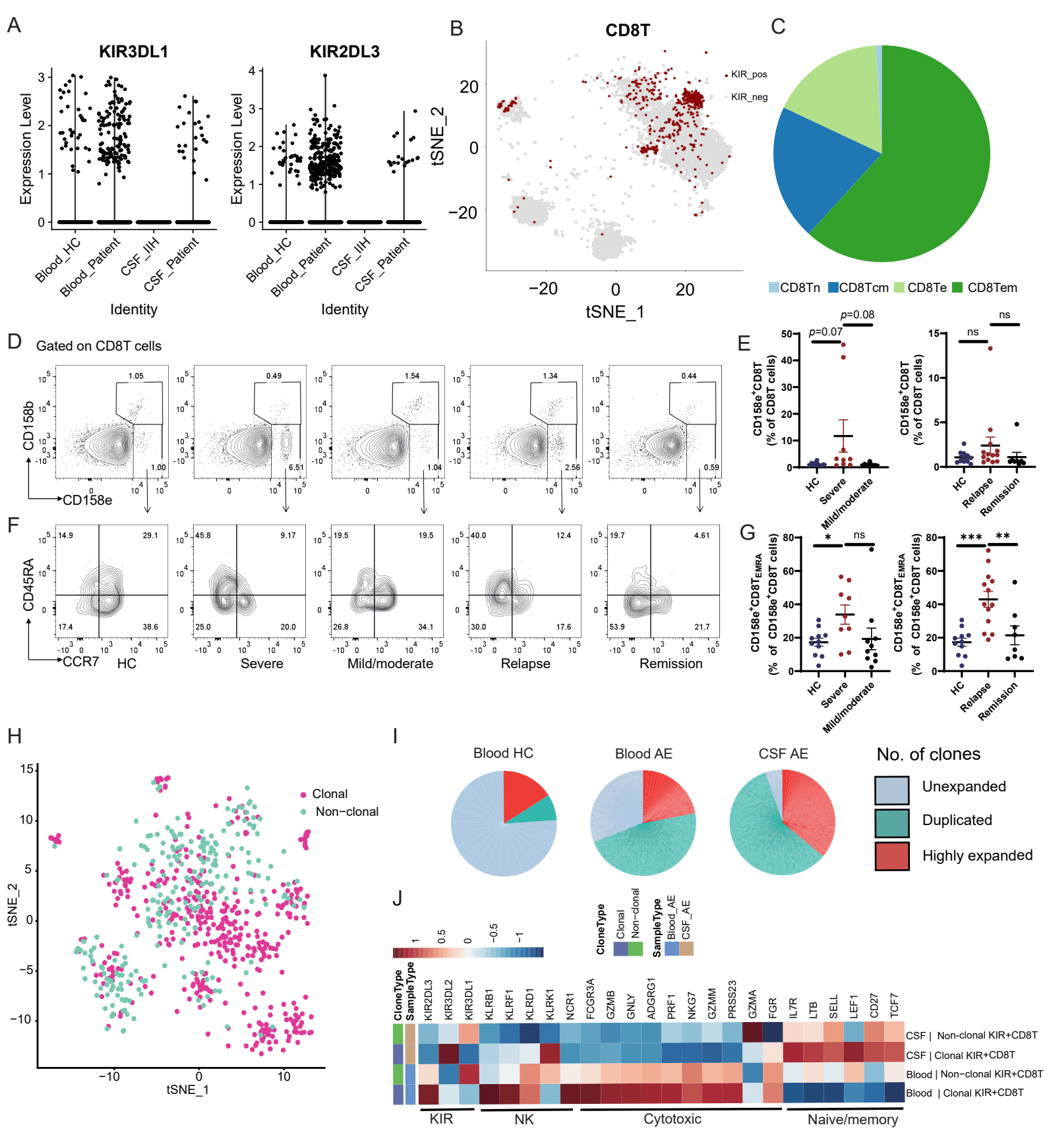
A
KIR3DL1
KIR2DL3
Expression Level
Blood_HC
Blood_Patient
CSF_IIH
CSF_Patient
Identity
B
CD8T
KIR_pos
KIR_neg
tSNE_1
tSNE_2
C
CD8Tn
CD8Tcm
CD8Te
CD8Tem
D
Gated on CD8T cells
CD158b
CD158e
E
CD158e+CD8T (% of CD8T cells)
p=0.07
p=0.08
ns
HC
Severe
Mild/moderate
Relapse
Remission
F
CD45RA
CCR7
G
CD158e+CD8TEMRA (% of CD158e+CD8T cells)
H
Clonal
Non−clonal
I
Blood HC
Blood AE
CSF AE
No. of clones
Unexpanded
Duplicated
Highly expanded
J
CloneType
SampleType
Clonal
Non−clonal
Blood_AE
CSF_AE
KIR2DL3
KIR3DL2
KIR3DL1
KLRB1
KLRF1
KLRD1
KLRK1
NCR1
FCGR3A
GZMB
GNLY
ADGRG1
PRF1
NKG7
GZMM
PRSS23
GZMA
FGR
IL7R
LTB
SELL
LEF1
CD27
TCF7
CSF | Non-clonal KIR+CD8T
CSF | Clonal KIR+CD8T
Blood | Non−clonal KIR+CD8T
Blood | Clonal KIR+CD8T
KIR
NK
Cytotoxic
Naive/memory

A Live Cell Imaging

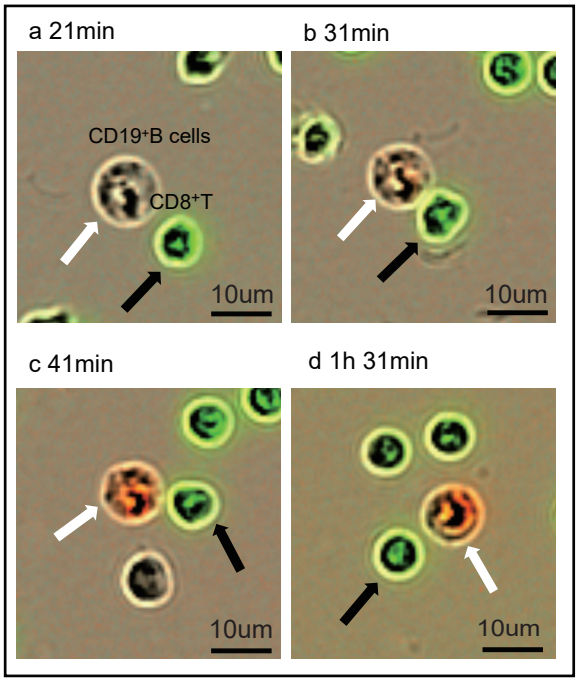

B Co-culture of CD8⁺T cells and B cells

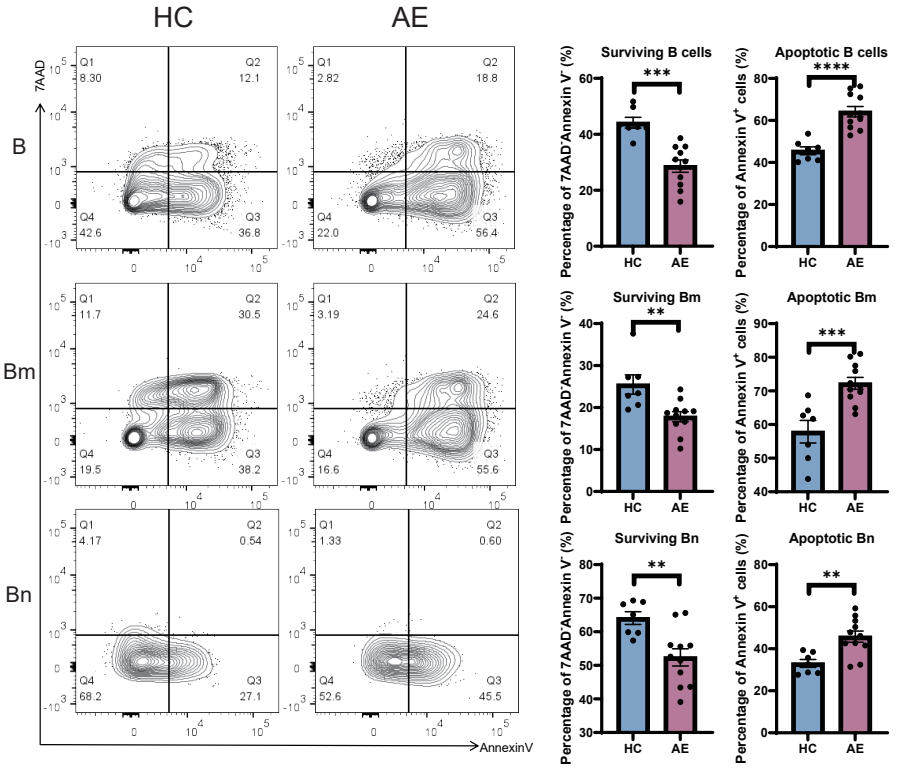

C

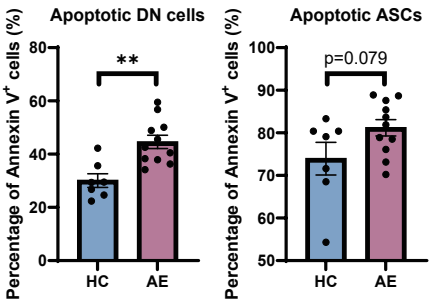

D Cell-cell interaction

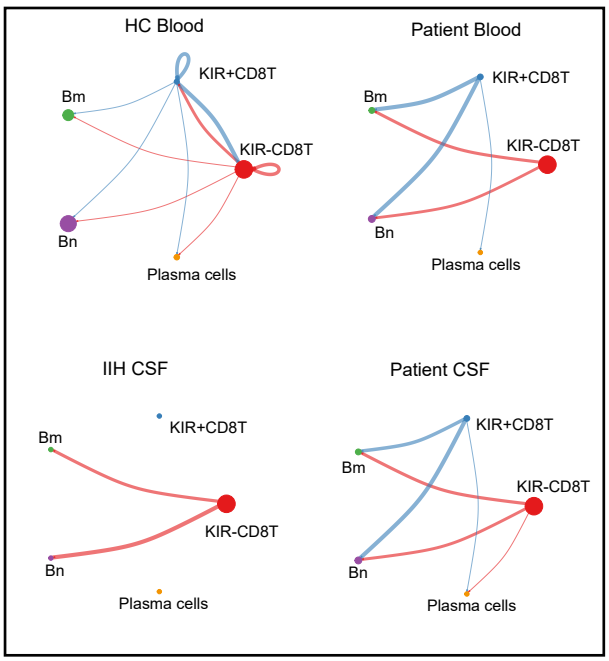
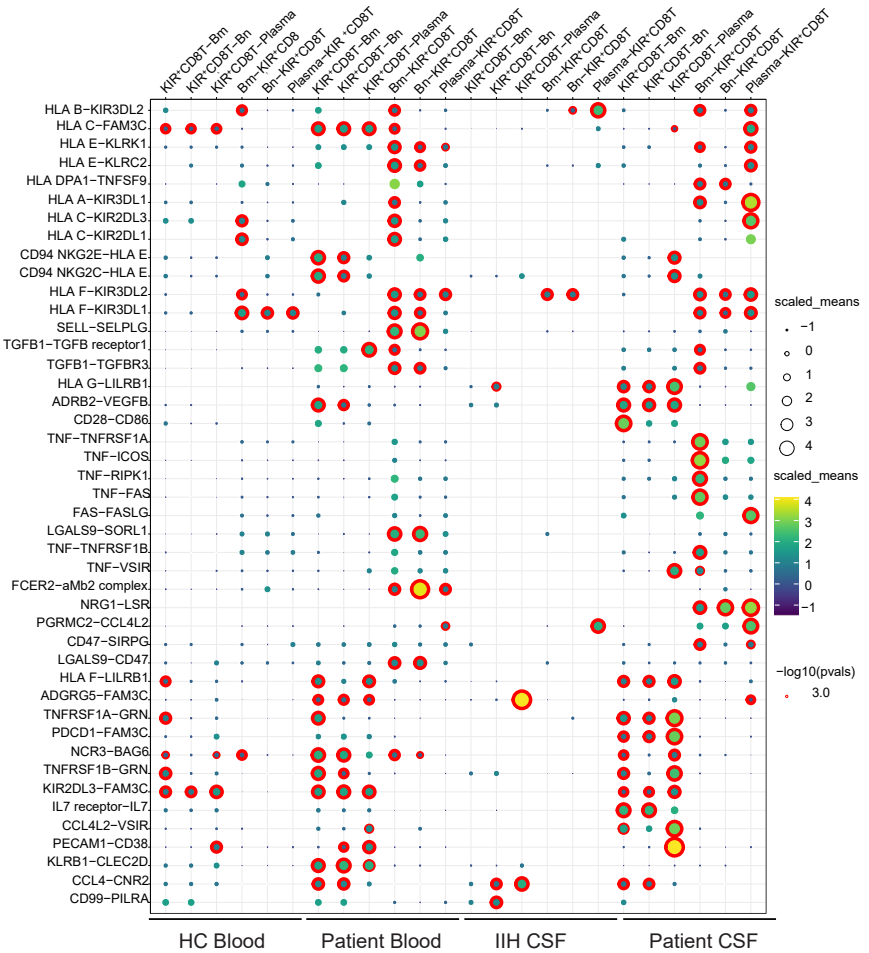
E Receptor-ligand pairing analysis